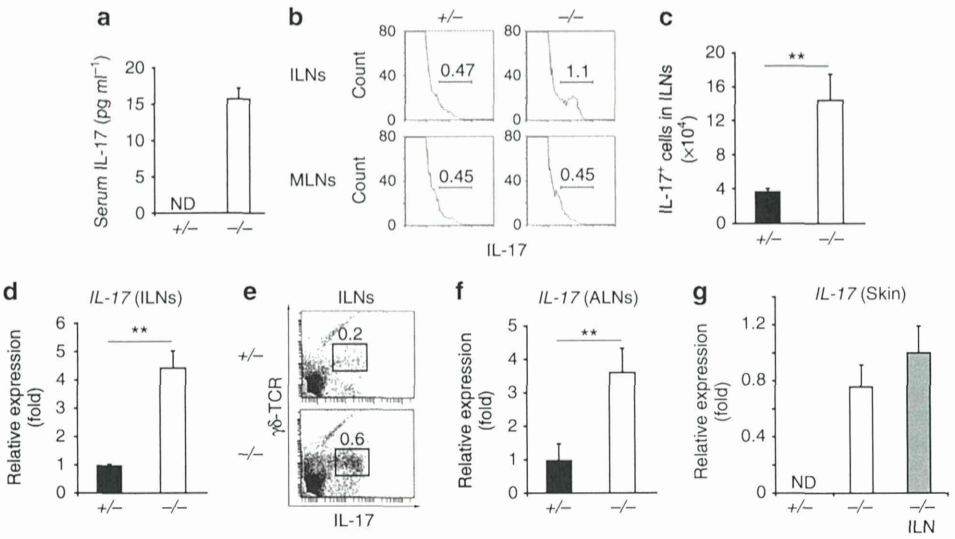

Figure 2 | Local and systemic IL-17 upregulation in *PLCδ1*$^{-/-}$ mice. (**a**) IL-17 concentration in the serum measured by ELISA. Mean±s.e.m. ($n=6$). (**b**) Representative FACS profiles of intracellular IL-17 in ILNs and MLNs. Cells were stimulated and intracellular IL-17 was detected ($n=6$ for ILNs and $n=3$ for MLNs). Three independent experiments were performed. (**c**) Absolute numbers of IL-17$^+$ cells in ILNs. Mean±s.e.m. ($n=6$). The combined results from three independent experiments are displayed. (**d**) *IL-17* mRNA expression in the ILNs determined by real-time RT-PCR. All values are normalized to *glyceraldehyde 3-phosphate dehydrogenase* (*GAPDH*). Results are displayed as arbitrary units (expression in *PLCδ1*$^{+/-}$ mice=1). Mean±s.e.m. ($n=3$). (**e**) Representative FACS profiles of γδ-TCR and intracellular IL-17 in ILNs ($n=3$). Cells were stimulated and intracellular IL-17 was detected. Three independent experiments were performed. (**f**) *IL-17* mRNA expression in the axillary lymph nodes (ALNs) determined by real-time RT-PCR. All values are normalized to *GAPDH*. Results are displayed as arbitrary units (expression in *PLCδ1*$^{+/-}$ mice=1). Mean±s.e.m. ($n=5$). (**g**) *IL-17* mRNA expression in skin determined by real-time RT-PCR. *PLCδ1*$^{-/-}$ ILN was used as the positive control for *IL-17* expression. All values are normalized to *GAPDH*. Results are displayed as arbitrary units (expression in *PLCδ1*$^{-/-}$ ILN=1). Mean±s.e.m. ($n=5$). Mice used in all experiments were 8–12 weeks old. Statistical significance was assessed using a Student's *t*-test. $^{**}P<0.01$. ND; not detected.

PLCδ1 produced *PLCδ1*$^{-/-}$ mice carrying *Foxn1::PLCδ1* (*Tg/KO* mice). PLCδ1 expression was restored in the skin of *Tg/KO* mice, but not in other organs such as the lungs, brain, ILNs, spleen and bone marrow (Fig. 3c). PLCδ1 protein was weakly expressed in *Tg/KO* thymuses, but these thymuses did not show obvious phenotypes, such as a disturbed balance of T-cell subtypes. Although the level of expression of PLCδ1 protein was somewhat lower in *Tg/KO* than in wild-type and heterozygous skin (Supplementary Fig. S8), the immunofluorescence observation indicated that both endogenous and transgene-derived PLCδ1 protein was expressed in suprabasal epidermis (Fig. 3d). These expression patterns were consistent with enriched expression of PLCδ1 and Foxn1 in differentiated keratinocytes[29,30]. At the histological level, the introduction of *Foxn1::PLCδ1* gene rescued epidermal hyperplasia and immune cell infiltration that were observed in *PLCδ1*$^{-/-}$ mice[20] (Fig. 3e,f). Importantly, *IL-17* expression was remarkably decreased in *Tg/KO* skin (Fig. 3g) compared with *PLCδ1*$^{-/-}$ skin. Residual expression of *IL-17* mRNA in *Tg/KO* skin may be caused by a lower level of PLCδ1 protein expression in *Tg/KO* than in control skin. *Tg/KO* mice showed no lymphadenopathy of the ILNs (Fig. 3h, Supplementary Table S2), and IL-17-producing cells were not increased in the ILNs in *Tg/KO* mice (Fig. 3i,j). Thus, reintroduction of *PLCδ1* into keratinocytes ameliorated local IL-17 upregulation. In addition, IL-17 concentrations in the serum of *Tg/KO* mice reverted to undetectable levels as in control mice (Fig. 3k), strongly suggesting that skin- and skin-draining lymph node-derived IL-17 was required for the elevation of IL-17 levels in serum. We also examined granulocyte populations in the peripheral blood, spleen, and bone marrow. Interestingly, *Tg/KO* mice did not exhibit granulocytosis (Fig. 3l), suggesting a close correlation between granulocytosis and IL-17 levels. These observations indicate that PLCδ1 expression in keratinocytes was sufficient for normal granulocyte counts and IL-17 levels in *PLCδ1*$^{-/-}$ mice.

Epidermal PLCδ1 regulates local and systemic IL-17 levels. We examined whether loss of PLCδ1 in keratinocytes caused IL-17 upregulation and granulocytosis by generating keratinocyte-specific conditional *PLCδ1*-knockout (*cKO*) mice with *K14* promoter-driven *Cre* transgenic mice (Fig. 4a,b). We confirmed that PLCδ1 was deleted in the epidermis of the *cKO* mice and that its expression was not altered in other organs such as the lungs, brain, ILNs, spleen, and bone marrow (Fig. 4c). As the *K14* promoter is active in the thymus, we examined the expression of PLCδ1 in the thymus, finding that PLCδ1 was downregulated in the thymus of *cKO* mice (Fig. 4c). However, we did not observe any obvious abnormalities in *cKO* thymus. *IL-17* was upregulated in the skin of *cKO* mice (Fig. 4d), whereas *interferon γ* and *IL-4* expression levels remained unchanged (Supplementary Fig. S7b). Interestingly, *IL-17* mRNA was upregulated more in the epidermis than in whole skin of *cKO* mice (Fig. 4e). CD3-positive T cells were major IL-17 producers in the *cKO* epidermis (Fig. 4f). The number of CD3-positive T cells was 1.7-fold higher in *cKO* than in control epidermis, suggesting that upregulation of *IL-17* mRNA in *cKO* epidermis is due, at least in part, to an increase in T cells. Further analysis revealed that *IL-17* was expressed by Vγ3-positive γδ T cells in *cKO* epidermis (Supplementary Fig. S9a). We also found that the level of *IL-17* mRNA was not significantly altered by depletion of Langerhans cells (Supplementary Fig. S9b). *cKO* mice also showed increased ILN size (Fig. 4g; Supplementary Table S3) and cell numbers (mean±s.e.m. cell numbers, $3.7\pm0.9\times10^6$ in controls versus $14\pm2.4\times10^6$ in *cKO* mice, both $n=6$). The number of IL-17-producing cells in the ILNs of *cKO* mice was more than six times that in the control mice (Fig. 4h).

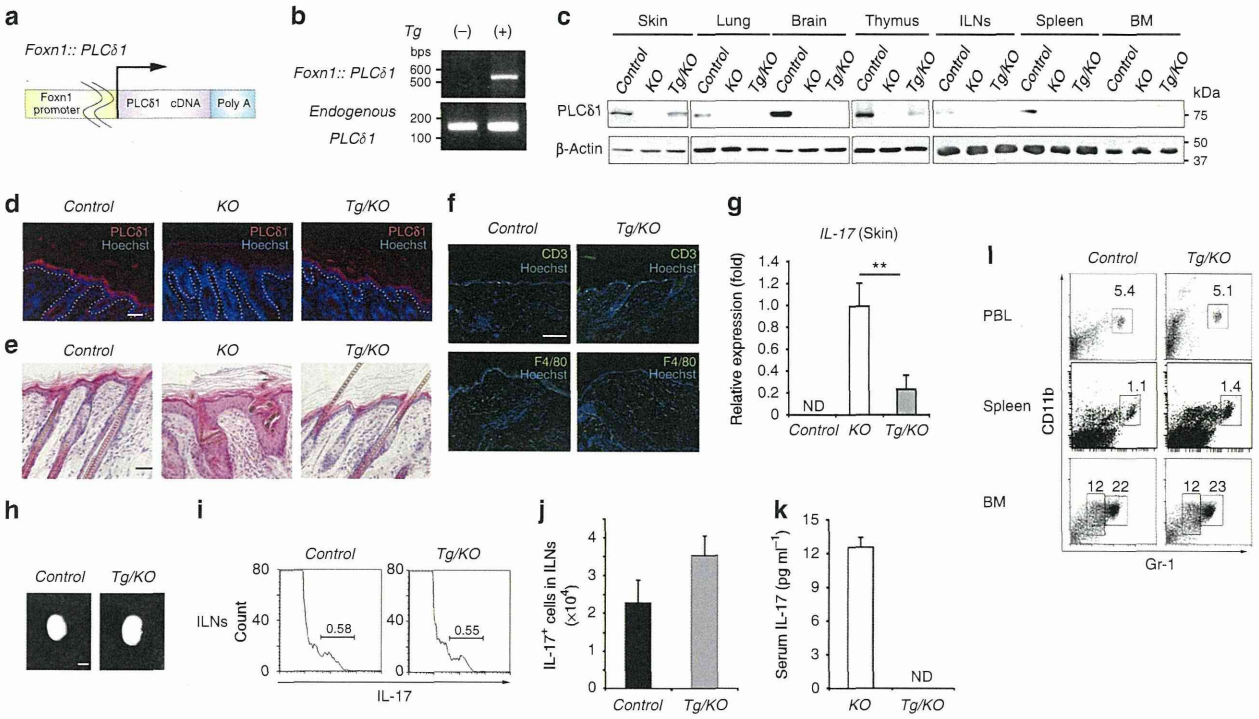

Figure 3 | Reintroduction of PLCδ1 in *PLCδ1*$^{-/-}$ keratinocytes restores normal IL-17 levels and granulocyte counts. (**a**) Structure of the *Foxn1::PLCδ1* gene. Poly A: the bovine growth hormone polyadenylation sequence. (**b**) PCR analysis of genomic DNA from the tails of *wild-type* and *Foxn1::PLCδ1* Tg mice. Products derived from *Foxn1::PLCδ1* and endogenous *PLCδ1*. (**c**) Immunoblotting of PLCδ1 and β-actin in tissues from control, *PLCδ1*$^{-/-}$ (*KO*), and *Tg/KO* mice. (**d**) Skin stained with antibody against PLCδ1 (red) and Hoechst stain (blue). Dotted lines denote the dermal-epidermal border. Scale bar, 50 μm. (**e**) Haematoxylin-eosin (HE) stained dorsal skin sections. Scale bar, 50 μm. (**f**) The skin was stained with antibodies against CD3 (green) or F4/80 (green) and Hoechst (blue). Scale bar, 100 μm. (**g**) *IL-17* mRNA expression in the skin of control, *PLCδ1*$^{-/-}$ (*KO*), and *Tg/KO* mice determined by real-time RT-PCR. All values are normalized to *GAPDH*. Results are displayed as arbitrary units (expression in the skin of *KO* mice = 1). Mean±s.e.m. ($n = 5$). (**h**) Macroscopic appearance of ILNs in control and *Tg/KO* mice. Scale bar, 1 mm. (**i**) Representative FACS profiles of intracellular IL-17 in ILNs. Cells were stimulated and intracellular IL-17 was detected ($n = 4$). Three independent experiments were performed. (**j**) Absolute numbers of IL-17$^+$ cells. Mean±s.e.m. ($n = 4$). The combined results from three independent experiments are displayed. (**k**) IL-17 concentration in serum measured by ELISA. Mean±s.e.m. ($n = 3$). (**l**) Representative FACS profiles of CD11b$^+$ Gr-1$^+$ granulocytes in the PBL, spleen, and BM of *Tg/KO* mice ($n = 4$). (**d**–**l**) 8–12-week-old mice were used. (**d**–**j**, **l**) Heterozygotes with *Foxn1::PLCδ1* were used as controls. Statistical significance was assessed using a Student's *t*-test. $^{**}P < 0.01$. ND, not detected.

The main IL-17-producing cells in *cKO* ILNs were γδ T cells (Fig. 4i). *IL-17* upregulation in ILNs of *cKO* mice was also confirmed by real-time RT–PCR (Fig. 4j). Production of the granulopoietic cytokine G-CSF is induced by IL-17 in many cell types, and we, therefore, examined whether conditioned medium (CM) derived from cKO skin-draining lymph nodes induced *G-CSF* expression. CM from *cKO* skin-draining lymph nodes induced higher *G-CSF* expression in fibroblasts compared with CM from control skin-draining lymph nodes (Fig. 4k). Importantly, CM from *cKO* skin-draining lymph nodes pretreated with anti-IL-17 neutralizing antibody did not cause *G-CSF* upregulation (Fig. 4k), strongly suggesting that cells in the *cKO* skin-draining lymph nodes secrete IL-17, leading to *G-CSF* production. If IL-17 derived from skin and skin-draining lymph nodes causes serum IL-17 elevation, then serum IL-17 concentrations should also be increased in *cKO* mice. Indeed, serum IL-17 levels were high in *cKO* mice (Fig. 4l), strongly suggesting that local IL-17 upregulation is linked to elevation of serum IL-17 levels. In addition, serum G-CSF concentrations were significantly increased in *cKO* mice compared with control mice (Fig. 4m). We further investigated the granulocyte population in *cKO* mice and found that *cKO* mice showed granulocytosis (Fig. 4n), consistent with local and serum IL-17 upregulation. Reduced numbers of bone marrow B lymphocytes and erythrocytes were also observed in *cKO* mice (Supplementary Fig. S10). Taken together, these results indicate that PLCδ1 in keratinocytes is required for the maintenance of normal IL-17 levels and granulocyte counts.

Epidermal PLCδ1 regulates IL-23 expression in the skin. We investigated the mechanisms of IL-17 upregulation in the epidermis by analysing the expression of the IL-17-inducing cytokine, IL-23. IL-23 and IL-12 are functionally related as heterodimeric cytokines that share the IL-12/23p40 subunit[31]. The mRNAs for the subunits of the IL-23 heterodimer (*IL-12/23p40* and *IL-23p19*) were upregulated in *cKO* skin (Fig. 5a), while *IL-12p35*, which encodes the IL-12-specific subunit, was not upregulated (Fig. 5a). In contrast, a dramatic decrease in *IL-23* expression was detected after reintroduction of PLCδ1 into keratinocytes (Supplementary Fig. S11). As *Tg/KO* skin showed no drastic increase in *IL-17* (Fig. 3g) whereas *cKO* skin showed remarkable *IL-17* upregulation (Fig. 4d), the expression level of *IL-23* was closely correlated with that of *IL-17* in skin. Similar to IL-17, IL-23p19 mRNA and protein were upregulated in cKO epidermis (Fig. 5b,c). Immunofluorescence experiments showed faint IL-23p19 immunoreactivity in control epidermis, whereas keratinocytes in the basal layer of *cKO* epidermis showed strong IL-23p19 immunoreactivity (Fig. 5d). *IL-23p19* expression was also assessed in primary keratinocyte cultures. *cKO* keratinocytes did not show

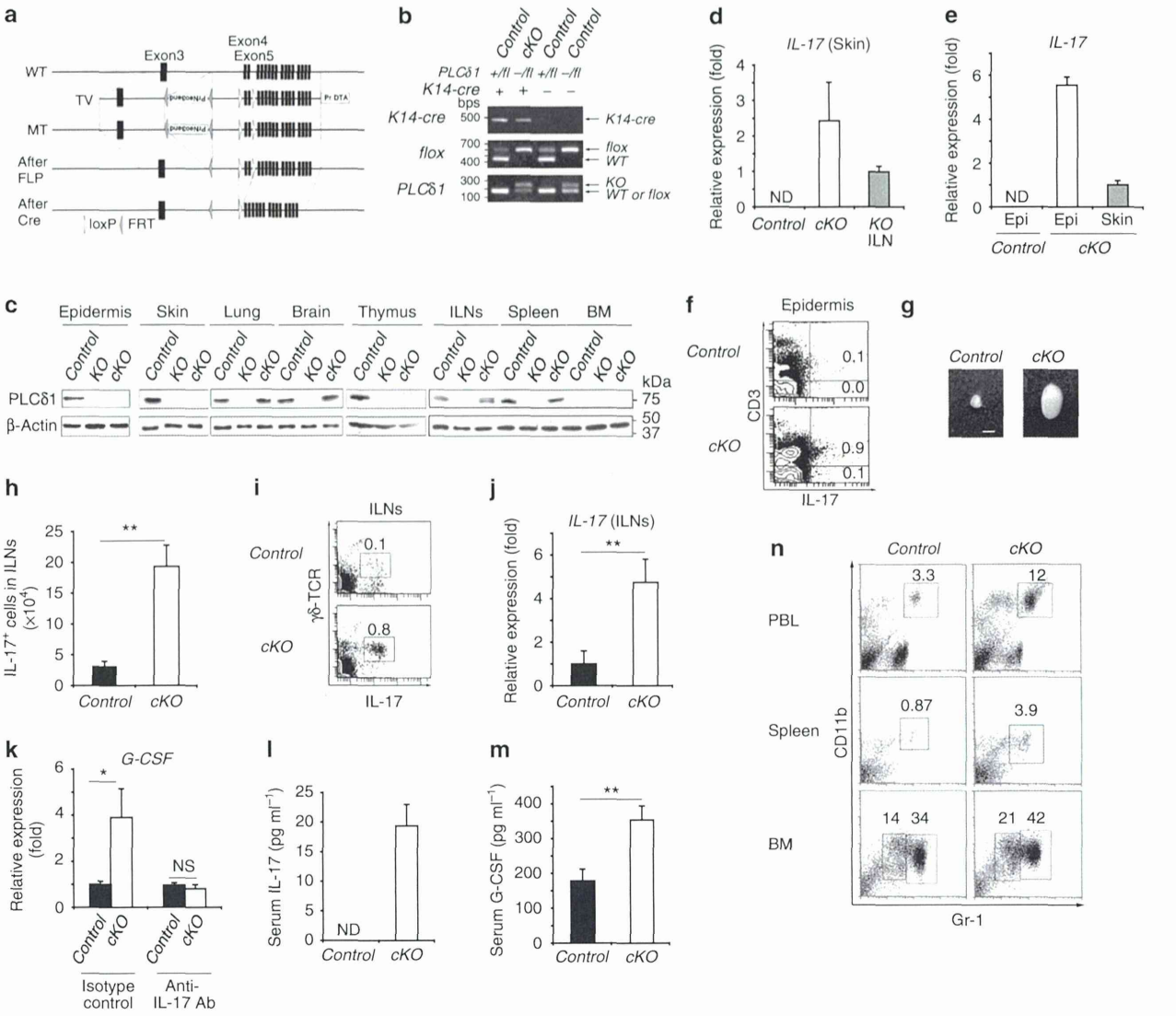

Figure 4 | Epidermal loss of PLCδ1 results in IL-17 upregulation and granulocytosis. (**a**) Genomic structure of the *PLCδ1* gene (WT). Exons are indicated by filled boxes. The structures of the targeting vector (TV) for disrupting the mouse *PLCδ1*, targeted allele (MT), allele after FLP recombination (After FLP), and allele after Cre recombination (After Cre) are displayed. (**b**) PCR genotyping of control and *cKO* mice. (**c**) Immunoblotting of PLCδ1 and β-actin in tissues from control, *PLCδ1*$^{-/-}$ (*KO*), and *cKO* mice. (**d**) *IL-17* mRNA expression in skin. *KO* ILN was used as positive control for *IL-17* expression. Results are displayed as arbitrary units (expression in *KO* ILN = 1). Mean±s.e.m. ($n = 3$). (**e**) *IL-17* mRNA expression in epidermis (epi) and whole skin (skin). Results are displayed as arbitrary units (expression in *cKO* whole skin = 1). Mean±s.e.m. ($n = 3$). (**f**) Representative FACS profiles of IL-17 and CD3 of epidermis ($n = 3$). Three independent experiments were performed. (**g**) Macroscopic appearance of ILNs. Scale bar = 2 mm. (**h**) Absolute numbers of IL-17$^+$ cells in ILNs. Mean±s.e.m. ($n = 6$). (**i**) Representative FACS profiles of γδ-TCR and intracellular IL-17 in ILNs ($n = 6$). Cells were stimulated. Five independent experiments were performed. (**j**) *IL-17* mRNA expression in the ILNs. Results are listed as arbitrary units (expression in control mice = 1). Mean±s.e.m. ($n = 3$). (**k**) *G-CSF* expression in Swiss 3T3 cells treated with skin-draining lymph-node CM in the presence of anti-IL-17 neutralizing antibody or isotype control. Results are displayed as arbitrary units (expression in cells treated with control skin-draining lymph-node CM and isotype control = 1). Mean± s.e.m. ($n = 4$). (**l**) IL-17 concentration in serum. Mean±s.e.m. ($n = 10$). (**m**) G-CSF concentration in the serum. Mean±s.e.m. ($n = 6$). (**n**) Representative FACS profiles of CD11b$^+$ Gr-1$^+$ granulocytes ($n = 8$). (**d**, **e**, **j**, **k**) All values are normalized to *GAPDH*. (**d**–**n**) 8–12-week-old mice were used. Statistical significance was assessed using a Student's *t*-test. $^*P < 0.05$; $^{**}P < 0.01$. ND, not detected.

increased expression of *IL-23p19*, regardless of their differentiation status (Fig. 5e). Thus, loss of PLCδ1 from keratinocytes did not upregulate *IL-23* in this *in vitro* system, suggesting that interactions between PLCδ1-deficient keratinocytes and other epidermal cells may be required for IL-23 production. We then examined whether the epidermal increase in IL-23 was linked to IL-17 upregulation in the *cKO* epidermis. IL-23 was neutralized using its specific p19 subunit antibody, and *IL-17* expression was then examined in control and *cKO* epidermal sheets. *IL-17* mRNA levels in the *cKO* epidermal sheet were clearly decreased in the presence of anti-IL-23p19 neutralizing antibody, compared with levels in the presence of isotype control (Fig. 5f), indicating that IL-23 has a critical role in *IL-17* upregulation in *cKO* epidermis. We then investigated the mechanisms responsible for IL-23 upregulation by assessing

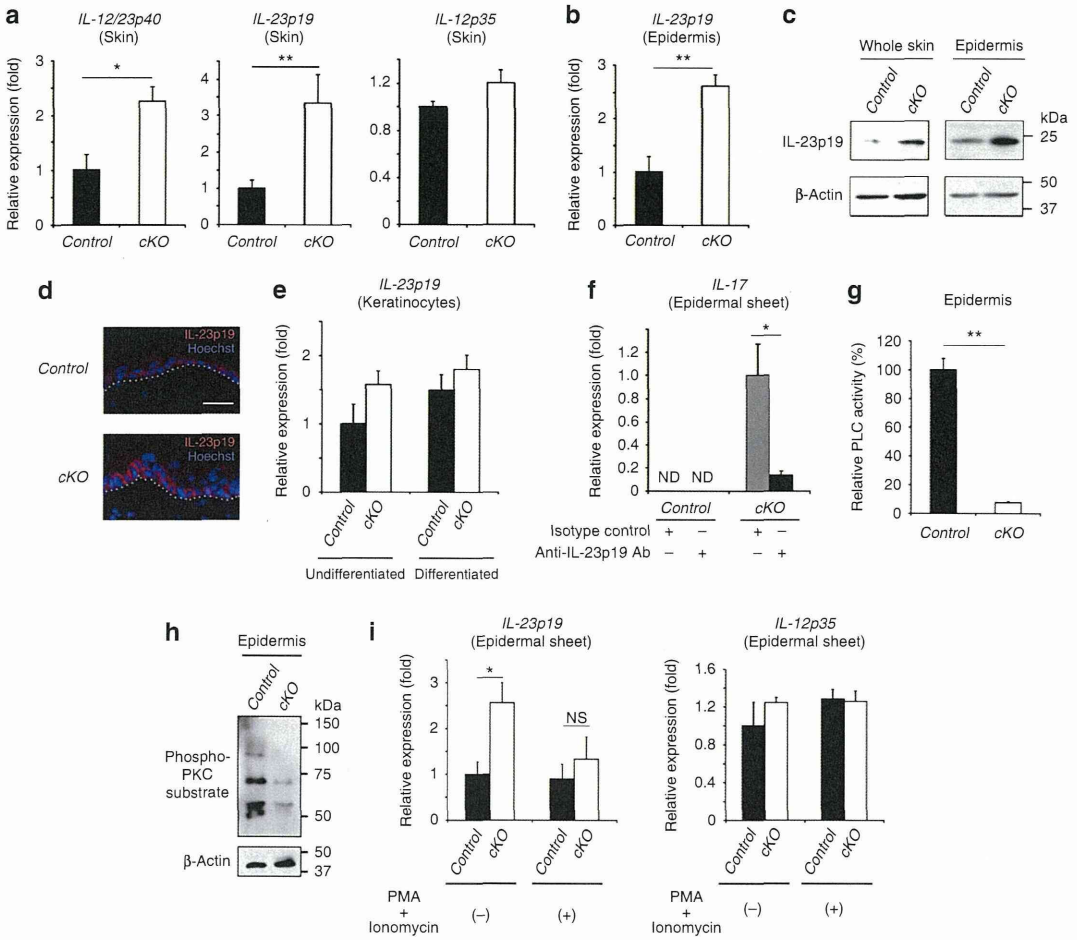

Figure 5 | IL-23 was upregulated in *cKO* skin. (**a**) *IL-12/23p40*, *IL-23p19*, and *IL-12p35* mRNA expression in the skin determined by real-time RT-PCR. All values are normalized to *GAPDH*. Results are displayed as arbitrary units (expression in control skin = 1). Mean ± s.e.m. ($n = 5$). (**b**) *IL-23p19* mRNA expression in epidermis determined by real-time RT-PCR. All values are normalized to *GAPDH*. Results are displayed as arbitrary units (expression in control = 1). Mean ± s.e.m. ($n = 6$). (**c**) Immunoblotting of IL-23p19 and β-actin in whole skin and epidermis from control and *cKO* mice. (**d**) Skin stained with the antibody against IL-23p19 (red) and Hoechst (blue). Dotted lines denote dermal-epidermal border. Scale bar, 30 μm. (**e**) *IL-23p19* mRNA expression in primary keratinocyte cultures determined by real-time RT-PCR. All values are normalized to *GAPDH*. Results are displayed as arbitrary units (expression in undifferentiated control keratinocytes = 1). Mean ± s.e.m. ($n = 3$). (**f**) Epidermal sheets were treated with anti-IL-23p19 neutralizing antibody or normal goat IgG, and *IL-17* mRNA expression was determined. All values are normalized to *GAPDH*. Results are displayed as arbitrary units (expression in *cKO* epidermal sheet treated with isotype control = 1). Mean ± s.e.m. ($n = 4$). (**g**) Relative PLC activity in epidermal lysates (PLC activity in control epidermis = 100%). Mean ± s.e.m. ($n = 4$). (**h**) Immunoblotting for phospho-PKC substrate in epidermis. β-actin was included as a loading control. (**i**) Epidermal sheets were treated with PMA and ionomycin, and mRNA expression of *IL-23p19* and *IL-12p35* was determined. All values are normalized to *GAPDH*. Results are displayed as arbitrary units (expression in control epidermal sheet without PMA/ionomycin treatment = 1). Mean ± s.e.m. ($n = 4$). Mice used in all experiments were 8–12 weeks old. Statistical significance was assessed using a Student's *t*-test. $^*P < 0.05$; $^{**}P < 0.01$. ND, not detected; NS, not significant.

activation of PLC and its downstream effector, PKC. We found that overall PLC activity was drastically decreased in *cKO* compared with control epidermis (Fig. 5g), indicating that, even in the presence of other PLC isoforms, loss of PLCδ1 impaired PLC activity in the epidermis. Consistent with the decrease in PLC activity, we found that the phosphorylation of PKC substrates was markedly decreased in cKO epidermis (Fig. 5h), indicating that loss of PLCδ1 from keratinocytes impaired the activation of the PLC downstream effector. We next determined whether the PLC downstream signal affected *IL-23* expression. PLC activation results in the generation of IP_3 and DAG, leading to elevated concentrations of intracellular calcium ions and activation of PKC. We, therefore, treated epidermal sheets with the calcium ionophore, ionomycin and phorbol 12-myristate 13-acetate (PMA), a synthetic analogue of DAG and a PKC activator, to mimic PLC activation. *IL-23p19* expression was upregulated in *cKO* epidermal sheets in the absence of ionomycin and PMA. Importantly, *IL-23p19* upregulation was ameliorated in *cKO* epidermal sheets in the presence of ionomycin and PMA (Fig. 5i). Expression of the IL-12-specific subunit, *IL-12p35*, was unchanged in the epidermis, regardless of the presence or absence of ionomycin and PMA (Fig. 5i). These results strongly suggest that *IL-23* upregulation in the *cKO* epidermis was caused by impaired PLC downstream signalling.

***cKO* skin shares features of human inflammatory skin diseases.** Because patients with human inflammatory skin diseases, such as psoriasis, show upregulation of IL-23 and IL-17 in the skin[8,32,33],

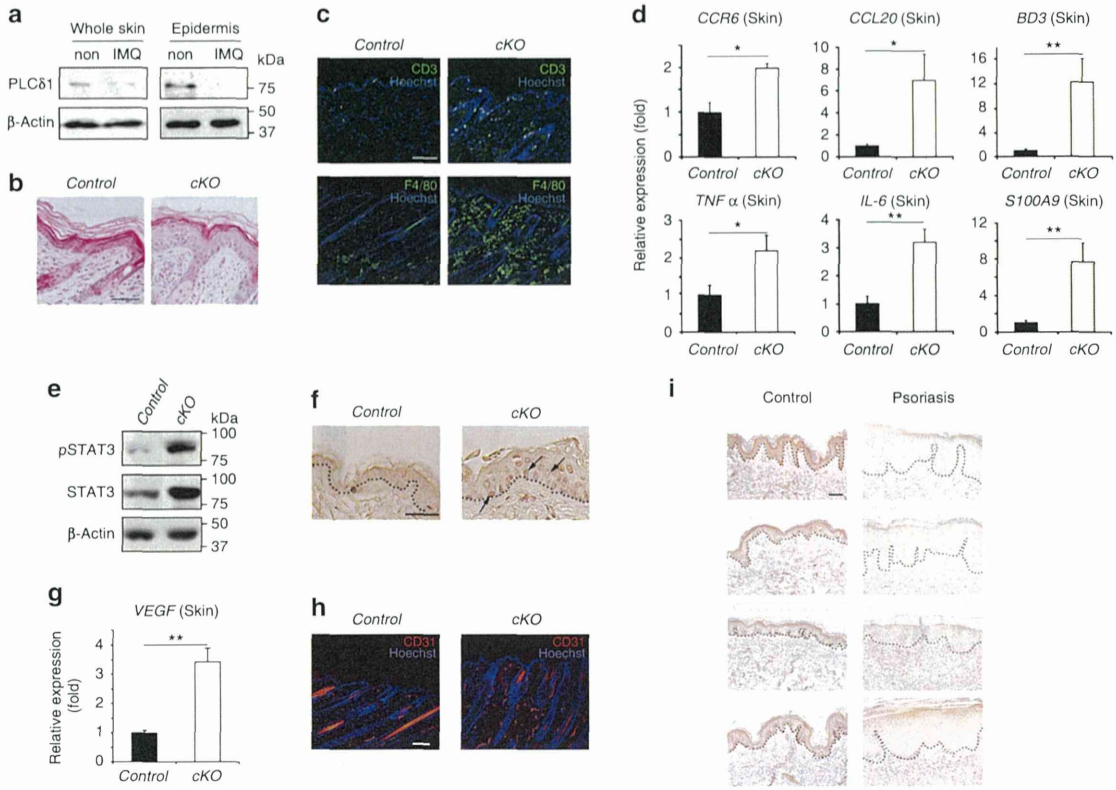

Figure 6 | *cKO* skin exhibits features of human inflammatory skin disease. (**a**) Immunoblotting of PLCδ1 and β-actin in whole skin or epidermis from non-treated (non) or IMQ-treated (IMQ) mice. (**b**) HE stained dorsal skin sections. Scale bar, 50 μm. The control skin has a normal epidermis, whereas the cKO skin has a thickened epidermis. (**c**) The skin was stained with antibodies against CD3 (green) or F4/80 (green) and Hoechst (blue). Scale bar,100 μm. (**d**) *CCR6*, *CCL20*, *β-defensin3* (*BD3*), *TNF α*, *IL-6*, and *S100A9* mRNA expression in skin determined by real-time RT-PCR. All values are normalized to *GAPDH*. Results are displayed as arbitrary units (expression in skin of control mice = 1). Mean ± s.e.m. ($n = 5$). (**e**) Immunoblotting for total and phosphorylated STAT3 (pSTAT3) in skin. β-actin was included as a loading control. (**f**) Skin stained with antibody against phosphorylated STAT3. Dotted lines denote dermal–epidermal border. Scale bar, 20 μm. Nuclear staining of phosphorylated STAT3 is indicated by arrows. (**g**) *VEGF* mRNA expression in skin determined by real-time RT-PCR. All values are normalized to *GAPDH*. Results are displayed as arbitrary units (expression in skin of control mice = 1). Mean ± s.e.m. ($n = 5$). (**h**) Skin stained with the antibody against CD31 (red) and Hoechst (blue). Hair shafts show nonspecific autofluorescence (red). Scale bar, 100 μm. (**i**) Skin from four non-psoriatic volunteers and four patients with psoriasis were stained with antibody against human PLCδ1 (brown). Dotted lines denote dermal–epidermal border. Scale bar, 100 μm. Body sites of each skin samples were as follows: control; arm, waist, back, and back (indicated from the top panel to the bottom panel). Psoriasis; arm, abdominal, leg, and leg (indicated from the top panel to the bottom panel). (**a**, **c**–**h**) 8–12-week-old mice were used. (**b**–**h**) Untreated IMQs were used. The data presented in (**b**, **c**, **e**, **f**, **h**) are representative of analyses of three mice per genotype. The data presented in (**a**) is representative of analyses of two mice per genotype. Statistical significance was assessed using a Student's *t*-test. $^{*}P < 0.05$; $^{**}P < 0.01$.

PLCδ1 could be involved in pathogenesis of these diseases. We therefore, examined PLCδ1 expression in the topical imiquimod (IMQ)-induced psoriasiform lesion, which is a mouse model of human psoriasis[34]. Interestingly, PLCδ1 protein was decreased in IMQ-treated skin compared with non-treated skin (Fig. 6a). PLCδ1 downregulation was also observed in the epidermis of IMQ-treated mice (Fig. 6a). These observations strongly suggest that epidermal PLCδ1 is implicated in a mouse model of human psoriasis. We next determined whether *cKO* skin shares features of human inflammatory skin diseases. Histological analysis revealed that *cKO* skin showed acanthosis (Fig. 6b) and infiltration of immune cells (Fig. 6c), as seen in human inflammatory skin diseases, such as psoriasis. In addition, *cKO* epidermis displayed abnormal patterns of differentiation marker expression, including the interfollicular expression of K6 (Supplementary Fig. S12), which is observed in human inflammatory skin diseases. Real-time RT–PCR showed that inflammatory genes upregulated in human inflammatory skin diseases are also upregulated in *cKO* skin (Fig. 6d)[35–40]. Activation of the signal transducer and activator of transcription 3 (STAT3) is also a feature of psoriasis[41], and western blotting revealed that both total and phosphorylated STAT3 proteins were increased in *cKO* skin (Fig. 6e). Consistent with these results, immunohistochemistry detected phosphorylated STAT3 in the nuclei of the *cKO* epidermis (Fig. 6f). Because the dermis is highly vascularized in some skin diseases[42–45], we analysed the expression levels of the potent angiogenic factor, *vascular endothelial growth factor (VEGF)*. *VEGF* upregulation was observed in *cKO* skin (Fig. 6g). In addition, immunofluorescence revealed that *cKO* skin was highly vascularized (Fig. 6h), in a manner similar to that in human inflammatory skin diseases. Most phenotypes in *cKO* skin were also observed in a mouse model of human psoriasis (Supplementary Fig. S13). Interestingly, PLCδ1 protein was downregulated in epidermis of human psoriatic skin (Fig. 6i). These observations strongly suggest that epidermal PLCδ1 is involved in human psoriasis.

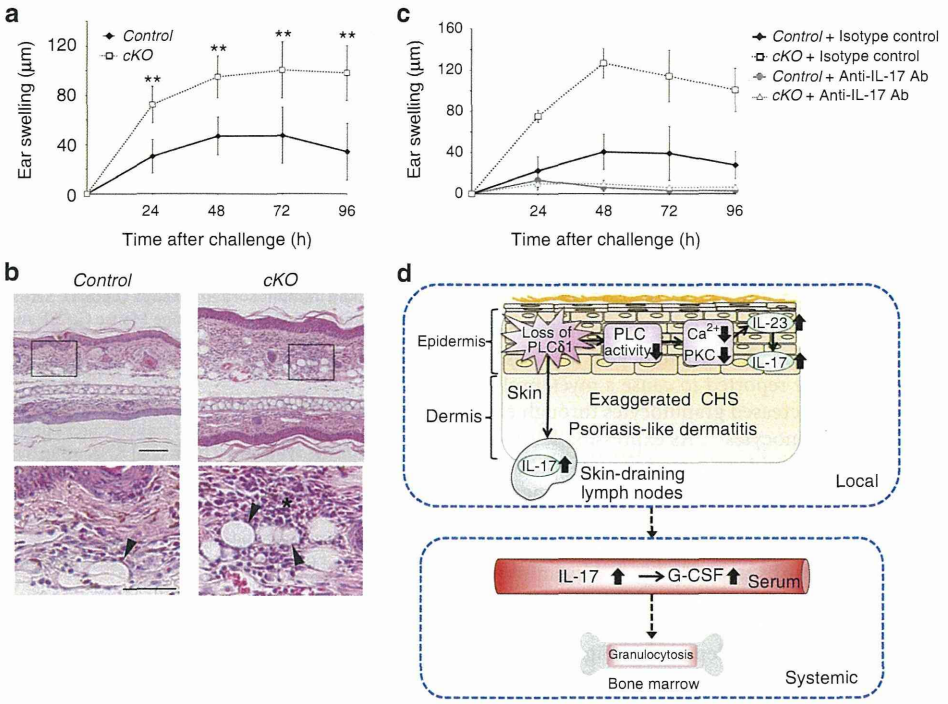

Figure 7 | Loss of PLCδ1 in keratinocytes exaggerates CHS responses. (**a**) Time course of ear swelling after DNFB challenge. Ear swelling was measured at the indicated times. Mean±s.d. ($n=4$). (**b**) HE stains of ear after DNFB challenge. The ears of sensitized mice were painted with DNFB, collected 96 h later and stained with HE. Lower panels are magnified views of the boxed regions in the upper panels. Scale bar in upper panel, 100 μm. Scale bar in lower panel,50 μm. (**c**) Sensitized mice were treated with anti-IL-17 neutralizing antibody or normal rat IgG before challenge, and ear swelling was measured at the indicated times. Mean±s.d. ($n=3$). Mice used in all experiments were 8-12 weeks old. The data presented in (**b**) are representative of three mice per genotype. Statistical significance was assessed using a Student's *t*-test. $^{**}P<0.01$. (**d**) Proposed model of local and systemic phenotypes induced by epidermal loss of PLCδ1. Epidermal loss of PLCδ1 impairs overall PLC activity and activation of PLC downstream signals, which causes increased production of IL-23 in the epidermis and whole skin. IL-23 induces IL-17 production in the epidermis. IL-17 was also overproduced in the skin-draining lymph nodes. This aberrant activation of the local IL-23/IL-17 axis resulted in a phenotype similar to that in human psoriasis and exaggerated CHS responses. Regarding systemic phenotypes, serum IL-17 levels were increased presumably as a result of skin and/or skin-draining lymph node-derived IL-17 (dotted arrow). Elevated serum IL-17 concentrations likely cause subsequent granulocytosis through G-CSF production (dotted arrow).

PLCδ1 in keratinocytes influences contact hypersensitivity. Dinitrofluorobenzene (DNFB)-induced contact hypersensitivity (CHS) of the skin in mice is commonly used as a model for studying the pathogenesis of allergic contact dermatitis (ACD), in which IL-17 has a critical role[4,46]. We, therefore, assessed CHS responses in *cKO* mice. Mice were sensitized and challenged with DNFB, and the CHS response was assessed by measuring ear swelling. On challenge with DNFB, DNFB-sensitized control mice exhibited a CHS response with mild ear swelling, whereas *cKO* mice showed more prominent ear swelling with exaggerated edema and severe inflammatory cell infiltration (Fig. 7a,b). Interestingly, IL-17 neutralization resulted in abrogation of the exaggerated ear swelling in *cKO* mice almost to basal level at any time after challenge (Fig. 7c). These results indicate that the exacerbated CHS in *cKO* mice was IL-17-dependent.

Discussion

In all of our mouse models, the level of expression of PLCδ1 in keratinocytes was inversely correlated with the levels of expression of IL-23 and IL-17 in skin and skin-draining LNs. Thus, loss of PLCδ1 in keratinocytes results in local activation of the IL-23/IL-17 axis (Fig. 7d). Keratinocytes from lesional psoriatic skin express IL-23 (ref. 32). In addition, human keratinocytes stimulated with nickel, a common hapten inducing CHS, produce IL-23 (ref. 47). These results are consistent with our observation that *IL-23p19* was upregulated in keratinocytes of cKO epidermis (Fig. 5d). Because IL-23p19 was upregulated mainly in basal layer of cKO interfollicular epidermis (Fig. 5d), essential and sufficient roles of suprabasal PLCδ1 in maintenance of normal IL-23p19 levels (Fig. 3d; Supplementary Fig. S11) is somewhat surprising. Interactions between suprabasal and basal keratinocytes might be important in regulation of IL-23p19 expression. We also found that γδ T cells in cKO epidermis expressed *IL-17* (Supplementary Fig. S9). Interestingly, γδ T cells were recently reported to be major IL-17 producers in skin of IL-23-mediated psoriasiform dermatitis[48,49].

Aberrant activation of the IL-23/IL-17 axis in the skin is known to be involved in the development of inflammatory human skin diseases, especially psoriasis[8]. Indeed, IL-23 injection into normal skin was sufficient for the development of psoriatic phenotypes in mice[50,51], and a monoclonal antibody against IL-12/23p40 subunit, ustekinumab is efficacious for the treatment of patients with moderate-to-severe psoriasis[52]. Although *cKO* skin shared some molecular features of psoriasis, it did not demonstrate all the histological characteristics of psoriatic skin. This may be because the expression of another key cytokine for the development of psoriasis, IL-22, was not upregulated in *cKO* skin (data not shown). Nonetheless, as PLCδ1 expression was decreased in the epidermis of patients with psoriasis (Fig. 6i) and in mouse IMQ-induced psoriasiform lesion (Fig. 6a), PLCδ1 may be involved in the pathogenesis of psoriasis. *cKO* mice also demonstrated increased sensitivity to hapten-induced

CHS, a mouse model of human ACD. The fact that the exaggerated CHS response in *cKO* mice was inhibited by IL-17 neutralization demonstrated the involvement of PLCδ1 in IL-17-mediated ACD.

Keratinocyte-specific ablation of PLCδ1 also caused systemic elevation of IL-17 and granulocytosis. Because activation of the local IL-23/IL-17 axis and systemic granulocytosis were both observed in *cKO*, but not in *Tg/KO* mice, the absence of epidermal PLCδ1, local IL-23/IL-17 axis activation, and systemic granulocytosis were strongly correlated with each other. This strict correlation strongly suggests that activation of the local IL-23/IL-17 axis and elevation of serum IL-17 and G-CSF concentrations are likely to be responsible for granulocytosis. On the basis of previous findings[53], the serum concentrations of IL-17 and G-CSF in *PLCδ1*$^{-/-}$ and *cKO* mice were sufficient to produce a systemic increase in granulocytes. The loss of JunB in keratinocytes was recently reported to cause a myeloproliferative disease characterized by increased granulocytes through elevated G-CSF production by keratinocytes[54]. As expression levels of *JunB* and *G-CSF* were unaltered in epidermis of *cKO* mice (data not shown), PLCδ1 seems to cause granulocytosis by a different mechanism to that observed in keratinocyte-specific *JunB*-knockout mice.

The results of this study demonstrate that disruption of the *PLCδ1* gene in keratinocytes disturbs not only local skin immune responses, but also the systemic homeostasis of haematopoietic cells, especially granulocytes. The proposed mechanism underlying the phenotypes seen in *cKO* mice is depicted in Fig. 7d. These findings suggest that targeting body-surface-specific inflammatory pathways may prevent not only inflammatory skin diseases but systemic granulocytosis and related disorders too.

Methods

Mice. *PLCδ1*$^{-/-}$ mice and *PLCδ1 flox/flox* mice (Acc. No. CDB0552K: http://www.cdb.riken.jp/arg/mutant%20mice%20list.html) were produced as described[55] (http://www.cdb.riken.jp/arg/Methods.html). In brief, a floxed allele of *PLCδ1* was generated by inserting loxP sites upstream of exon 4 and downstream of exon 5. The resulting mutant mice carrying the floxed allele of *PLCδ1* were crossed with *B6-Tg (CAG-FLPe)36* mice (RIKEN BRC, RBRCO 1834) to remove the neomycin-resistant cassette, and then with K14-Cre transgenic mice[56] (#004782, Jackson Laboratory, Bar Harbor, ME, USA) to remove the floxed exons. *Foxn1::PLCδ1* transgenic mice (Acc. No. CDB0437T: http://www.cdb.riken.jp/arg/TG%20mutant%20mice%20list.html) were developed as per a standard protocol. In brief, murine *PLCδ1* was subcloned into a plasmid that contained a 27,970-bp *Foxn1* promoter fragment (gift from Dr T. Boehm)[57]. The construct was linearized and injected into C57BL/6N or BDF1 pronuclei according to standard protocols. *Tg/KO* mice were generated with two independent transgenic mouse lines. Adult mice or pups were routinely genotyped by PCR. The primer sequences used are listed in Supplementary Table S4. Age- and sex-matched littermates were used to minimize any effects of genetic background. All animal studies were approved by the animal experiments review board of Tokyo University of Pharmacy and Life Sciences.

FACS analysis of cells from peripheral blood and tissues. Fluorophor-conjugated monoclonal antibodies were used in various combinations to stain peripheral blood mononuclear cells, splenocytes, and bone marrow. Red blood cells were depleted with 1×RBC Lysis Buffer (eBioscience, San Diego, CA, USA). For staining, 2–5×10^6 cells were used. Fc receptor was blocked by CD16/32 antibody. After staining (Supplementary Table S5), the cells were fixed with 1% paraformaldehyde. Stained and fixed cells were assayed using a FACSCanto flow cytometer (BD Biosciences) and further analysed with FlowJo software (Tree Star, Ashland, OR, USA).

BrdU incorporation assay. Analysis of *in vivo* BrdU incorporation into immature granulocytes was performed using the BrdU Flow Kit (BD Pharmingen) after intraperitoneal injection of 1.5 mg of BrdU. Mice were killed 1 h later and the bone marrow cells were collected. Cell surface markers were identified using Gr-1 and CD11b antibodies.

Colony-forming unit assays. Colony-forming cell assays were performed using bone marrow cells and MethoCult M3434 (Stem Cell Technologies, Vancouver, British Columbia, Canada). Colonies were counted after 12 days' incubation in a humidified atmosphere with 5% CO_2 and characterized according to their unique morphologies.

Bone marrow transplantation. Recipient mice were irradiated with 9 Gy whole-body irradiation. Donors were *PLCδ1*$^{+/-}$ or *PLCδ1*$^{-/-}$ (CD45.2$^+$) mice, while recipients were of B6.SJL (CD45.1$^+$) background. A total of 4×10^6 donor bone marrow cells were intravenously injected into each recipient. Peripheral blood, spleen, and bone marrow chimerism were analysed by immunostaining for CD45 congenic marker isoforms in leukocytes 1 month after transplantation.

Intracellular IL-17 staining. Cells from ILNs and MLNs were cultured for 4 h in RPMI-1640 (Invitrogen) containing 10% fetal bovine serum (FBS) in the presence of PMA (50 ng ml^{-1}; Sigma) and ionomycin (1 μg ml^{-1}; Invitrogen). Brefeldin A (10 μg ml^{-1}; Sigma) was added for the last 2 h of incubation. Cells were collected and stained with antibodies (Supplementary Table S5) against cell surface antigens. The cells were then subjected to intracellular cytokine staining using the mouse Foxp3 buffer set (BD Pharmingen), according to the manufacturer's instructions.

Enzyme-linked immunosorbent assays (ELISA). Serum G-CSF and IL-17 levels were determined using the Quantikine Mouse G-CSF and IL-17 Immunoassay kits (R&D Systems, Minneapolis, MN, USA), respectively, according to the manufacturer's instructions.

Real-time RT–PCR. Total RNA was isolated using the RNeasy Mini kit (Qiagen, Hilden, Germany), according to the manufacturer's protocol. Template complementary DNA was synthesized from total RNA using the QuantiTect Reverse Transcription kit (Qiagen) or the ReverTra Ace qPCR RT kit (Toyobo, Osaka, Japan). Real-time PCR was performed using the THUNDERBIRD SYBR qPCR Mix (Toyobo) in a CFX96 thermocycler (Bio-Rad, München, Germany). Primer sequences are listed in Supplementary Table S4. The relative amounts of mRNA were normalized to glyceraldehyde 3-phosphate dehydrogenase mRNA.

Immunofluorescence and immunohistochemistry. Immunofluorescence analysis for IL-23p19, CD3, F4/80, CD31, K1, K5, K6, and Loricrin was performed using frozen sections. Briefly, sections were fixed in acetone (for IL-23p19) or 2% paraformaldehyde (for CD3, F4/80, CD31, K1, K5, K6 and Loricrin), and nonspecific binding sites were blocked with TNB (PerkinElmer, Waltham, MA, USA). The sections were then incubated with primary antibodies (Supplementary Table S5). Antibody binding was detected by subsequent incubation of the sections with Alexa Fluor 488 or 568-conjugated secondary antibody. Counter-staining was performed with Hoechst 33258 (Invitrogen). Immunofluorescence analysis of mouse PLCδ1 was performed using paraffin sections with TSA Plus Cyanine 3 System (PerkinElmer). Sections were observed under a BZ-8000 microscope (Keyence, Tokyo, Japan). Immunohistochemistry for phosphorylated STAT3 was carried out on paraffin sections, according to the manufacturer's instructions. Immunohistochemical assays for human PLCδ1 were performed using paraffin sections with a Vectastain Elite rabbit ABC kit (Vector Laboratories, Burlingame, CA, USA). Sections were examined under a BX51 microscope (Olympus, Tokyo, Japan).

Measurement of PLC activity. Epidermis was homogenized in 40 mM HEPES-KOH, pH 7.0, 120 mM KCl containing 0.1% sodium deoxycholate. The PLC activity of these epidermal lysates was assayed by hydrolysis of $PI(4,5)P_2$ in a 50-μl reaction mixture containing 20,000 d.p.m. of [3H]PI(4,5)P2 (PerkinElmer Life Sciences), 40 μM $PI(4,5)P_2$, and 50 μM phosphatidylethanolamine as phospholipids micelles. The micelles were incubated with epidermal lystaes at 37 °C for 5 min, and the reaction was stopped by adding chloroform/methanol (2:1, v/v). Radioactive IP_3 was extracted with 1 N HCl, and radioactivity in the upper aqueous phase was measured for 1 min in a liquid scintillation counter[58].

Hapten-induced CHS. Mice were sensitized with DNFB (Sigma) by painting the shaved dorsal skin with 50 μl of 0.5% (w/v) DNFB dissolved in acetone:olive oil (4:1). Five days later, 10 μl of 0.2% (w/v) DNFB was applied to both sides of the right ear. The same volume of acetone:olive oil (4:1) was applied to the left ear as an unchallenged control. Ear swelling was calculated by subtracting the thickness of the left ear from that of the right ear after measurement with a pair of callipers. To detect the role of IL-17 in the elicitation of CHS, mice were sensitized and treated twice intraperitoneally with anti-IL-17 antibody (R&D Systems) (200 μg per mouse) or normal rat IgG (R&D Systems) (200 μg per mouse) on days 4 and 5, after sensitization. Mice were challenged on day 5 and CHS was measured.

Explant culture of epidermal sheet. Ear or tail skin was removed from adult mice and incubated for 30 min at 37 °C in 0.25% trypsin (Invitrogen) to separate the epidermis from the dermis. For stimulation with PMA and ionomycin, epidermal sheets were cultured for 6 h in RPMI-1640 containing 10% FBS with or without PMA (100 ng ml^{-1}) and ionomycin (2.5 μg ml^{-1}). For IL-23 neutralization, epidermal sheets were cultured for 24 h in RPMI-1640 containing 10% FBS with 4 μg of anti-IL-23p19 antibody (R&D Systems) or normal goat IgG (R&D Systems).

G-CSF induction. Swiss 3T3 cells were maintained in DMEM containing 10% FBS. Cells isolated from skin-draining lymph nodes were cultured for 48 h in RPMI-1640 containing 10% FBS and CM was collected. Swiss 3T3 cells were cultured for 24 h in DMEM containing 10% FBS and skin-draining lymph-node CM. Skin-draining lymph-node CM was preincubated with anti-IL-17 antibody (1 μg ml^{-1}) or normal rat IgG for 1 h before adding to Swiss 3T3 cells.

Intracellular IL-17 staining of epidermal single-cell preparation. Ear skin was removed from adult mice and incubated for 1 h at 37 °C in 0.5% trypsin to separate the epidermis from the dermis. Single-cell suspensions were prepared from the epidermis by incubation for an additional 15 min with 0.5% trypsin. Leukocyte enrichment was performed by overlaying a single-cell suspension on a Percoll density gradient and centrifuging. Epidermal cell suspensions were then stained with antibodies against CD3, and the cells were subjected to intracellular IL-17 staining using the mouse Foxp3 buffer set, according to the manufacturer's instructions.

IMQ treatment. Balb/c mice were treated on the shaved back skin or inner side of the right ear with a daily topical dose of 62.5 or 12.5 mg of commercially available IMQ cream (5%) (Beselna Cream; Mochida Pharmaceuticals, Tokyo, Japan) for 6 days, respectively. Left ears were untreated and used as control. Back skin or ears were collected 24 h after the last treatment. For the preparation of epidermal samples, ear skin was incubated for 30 min at 37 °C in 0.25% trypsin to separate the epidermis from the dermis.

Human subjects. Patients with psoriasis and healthy volunteers without psoriasis were enrolled. Informed consent was obtained from all participants. The study protocol was approved by the Ethics Committee of Kyoto University and was conducted according to the Declaration of Helsinki Principles. Skin biopsies were analysed by immunohistochemistry.

References

1. Berridge, M. J. & Irvine, R. F. Inositol trisphosphate, a novel second messenger in cellular signal transduction. *Nature* **312,** 315–321 (1984).
2. Nishizuka, Y. The molecular heterogeneity of protein kinase C and its implications for cellular regulation. *Nature* **334,** 661–665 (1988).
3. Suh, P. G. *et al.* Multiple roles of phosphoinositide-specific phospholipase C isozymes. *BMB Rep.* **41,** 415–434 (2008).
4. Nakae, S. *et al.* Antigen-specific T cell sensitization is impaired in IL-17-deficient mice, causing suppression of allergic cellular and humoral responses. *Immunity* **17,** 375–387 (2002).
5. Goverman, J. Autoimmune T cell responses in the central nervous system. *Nat. Rev. Immunol.* **9,** 393–407 (2009).
6. Lubberts, E. *et al.* Requirement of IL-17 receptor signaling in radiation-resistant cells in the joint for full progression of destructive synovitis. *J. Immunol.* **175,** 3360–3368 (2005).
7. Nakae, S., Nambu, A., Sudo, K. & Iwakura, Y. Suppression of immune induction of collagen-induced arthritis in IL-17-deficient mice. *J. Immunol.* **171,** 6173–6177 (2003).
8. Lee, E. *et al.* Increased expression of interleukin 23 p19 and p40 in lesional skin of patients with psoriasis vulgaris. *J. Exp. Med.* **199,** 125–130 (2004).
9. Fujino, S. *et al.* Increased expression of interleukin 17 in inflammatory bowel disease. *GUT* **52,** 65–70 (2003).
10. Yen, D. *et al.* IL-23 is essential for T cell-mediated colitis and promotes inflammation via IL-17 and IL-6. *J. Clin. Invest.* **116,** 1310–1316 (2006).
11. Aggarwal, S., Ghilardi, N., Xie, M. H., de Sauvage, F. J. & Gurney, A. L. Interleukin-23 promotes a distinct CD4 T cell activation state characterized by the production of interleukin-17. *J. Biol. Chem.* **278,** 1910–1914 (2003).
12. Happel, K. I. *et al.* Roles of Toll-like receptor 4 and IL-23 in IL-17 expression in response to Klebsiella pneumoniae infection. *J. Immunol.* **170,** 4432–4436 (2003).
13. Forlow, S. B. *et al.* Increased granulopoiesis through interleukin-17 and granulocyte colony-stimulating factor in leukocyte adhesion molecule-deficient mice. *Blood* **98,** 3309–3314 (2001).
14. Schwarzenberger, P. *et al.* IL-17 stimulates granulopoiesis in mice: use of an alternate, novel gene therapy-derived method for *in vivo* evaluation of cytokines. *J. Immunol.* **161,** 6383–6389 (1998).
15. Schwarzenberger, P. *et al.* Requirement of endogenous stem cell factor and granulocyte-colony-stimulating factor for IL-17-mediated granulopoiesis. *J. Immunol.* **164,** 4783–4789 (2000).
16. Fried, L. *et al.* Inflammatory and prothrombotic markers and the progression of renal disease in elderly individuals. *J. Am. Soc. Nephrol.* **15,** 3184–3191 (2004).
17. Margolis, K. L. *et al.* Leukocyte count as a predictor of cardiovascular events and mortality in postmenopausal women: the Women's Health Initiative Observational Study. *Arch. Intern. Med.* **165,** 500–508 (2005).
18. Ruggiero, C. *et al.* White blood cell count and mortality in the Baltimore Longitudinal Study of Aging. *J. Am. Coll. Cardiol.* **49,** 1841–1850 (2007).
19. Nakamura, Y. *et al.* Phospholipase C-δ1 and -δ3 are essential in the trophoblast for placental development. *Mol. Cell. Biol.* **25,** 10979–10988 (2005).
20. Ichinohe, M. *et al.* Lack of phospholipase C-delta1 induces skin inflammation. *Biochem. Biophys. Res. Commun.* **356,** 912–918 (2007).
21. Swamy, M., Jamora, C., Havran, W. & Hayday, A. Epithelial decision makers: in search of the 'epimmunome'. *Nat. Immunol.* **11,** 656–665 (2010).
22. Nestle, F. O., Di Meglio, P., Qin, J. Z. & Nickoloff, B. J. Skin immune sentinels in health and disease. *Nat. Rev. Immunol.* **9,** 679–691 (2009).
23. Xiao, W. *et al.* Tumor suppression by phospholipase C-β3 via SHP-1-mediated dephosphorylation of Stat5. *Cancer Cell* **16,** 161–171 (2009).
24. Guo, Y., Rebecchi, M. & Scarlata, S. Phospholipase Cbeta2 binds to and inhibits phospholipase Cdelta1. *J. Biol. Chem.* **280,** 1438–1447 (2005).
25. Ueda, Y., Kondo, M. & Kelsoe, G. Inflammation and the reciprocal production of granulocytes and lymphocytes in bone marrow. *J. Exp. Med.* **201,** 1771–1780 (2005).
26. Walkley, C. R. *et al.* A microenvironment-induced myeloproliferative syndrome caused by retinoic acid receptor gamma deficiency. *Cell* **129,** 1097–1110 (2007).
27. Yang, L. *et al.* Cdc42 critically regulates the balance between myelopoiesis and erythropoiesis. *Blood* **110,** 3853–3861 (2007).
28. Walkley, C. R., Yuan, Y. D., Chandraratna, R. A. & McArthur, G. A. Retinoic acid receptor antagonism *in vivo* expands the numbers of precursor cells during granulopoiesis. *Leukemia* **16,** 1763–1772 (2002).
29. Nakamura, Y. *et al.* Phospholipase C-δ1 is an essential molecule downstream of Foxn1, the gene responsible for the nude mutation, in normal hair development. *FASEB J.* **22,** 841–849 (2008).
30. Lee, D., Prowse, D. M. & Brissette, J. L. Association between mouse nude gene expression and the initiation of epithelial terminal differentiation. *Dev. Biol.* **208,** 362–374 (1999).
31. Oppmann, B. *et al.* Novel p19 protein engages IL-12p40 to form a cytokine, IL-23, with biological activities similar as well as distinct from IL-12. *Immunity* **13,** 715–725 (2000).
32. Johansen, C. *et al.* Characterization of the interleukin-17 isoforms and receptors in lesional psoriatic skin. *Br. J. Dermatol.* **160,** 319–324 (2009).
33. Piskin, G., Sylva-Steenland, R. M., Bos, J. D. & Teunissen, M. B. *In vitro* and *in situ* expression of IL-23 by keratinocytes in healthy skin and psoriasis lesions: enhanced expression in psoriatic skin. *J. Immunol.* **176,** 1908–1915 (2006).
34. van der Fits, L. *et al.* Imiquimod-induced psoriasis-like skin inflammation in mice is mediated via the IL-23/IL-17 axis. *J Immunol.* **182,** 5836–5845 (2009).
35. Homey, B. *et al.* Up-regulation of macrophage inflammatory protein-3 alpha/CCL20 and CC chemokine receptor 6 in psoriasis. *J. Immunol.* **164,** 6621–6632 (2000).
36. Ong, P. Y. *et al.* Endogenous antimicrobial peptides and skin infections in atopic dermatitis. *N. Engl. J. Med.* **347,** 1151–1160 (2002).
37. Wilson, N. J. *et al.* Development, cytokine profile and function of human interleukin 17-producing helper T cells. *Nat. Immunol.* **8,** 950–957 (2007).
38. Ettehadi, P. *et al.* Elevated tumour necrosis factor-alpha (TNF-alpha) biological activity in psoriatic skin lesions. *Clin. Exp. Immunol.* **96,** 146–151 (1994).
39. Grossman, R. M. *et al.* Interleukin 6 is expressed in high levels in psoriatic skin and stimulates proliferation of cultured human keratinocytes. *Proc. Natl Acad. Sci. USA* **86,** 6367–6371 (1989).
40. Broome, A. M., Ryan, D. & Eckert, R. L. S100 protein subcellular localization during epidermal differentiation and psoriasis. *J. Histochem. Cytochem.* **51,** 675–685 (2003).
41. Sano, S. *et al.* Stat3 links activated keratinocytes and immunocytes required for development of psoriasis in a novel transgenic mouse model. *Nat. Med.* **11,** 43–49 (2005).
42. Creamer, D., Allen, M. H., Sousa, A., Poston, R. & Barke, J. N. Localization of endothelial proliferation and microvascular expansion in active plaque psoriasis. *Br. J. Dermatol.* **136,** 859–865 (1997).
43. Hern, S., Stanton, A. W., Mellor, R., Levick, J. R. & Mortimer, P. S. Control of cutaneous blood vessels in psoriatic plaques. *J. Invest. Dermatol.* **113,** 127–132 (1999).
44. Murphy, M., Kerr, P. & Grant-Kels, J. M. The histopathologic spectrum of psoriasis. *Clin. Dermatol.* **25,** 524–528 (2007).
45. Micali, G., Lacarrubba, F., Musumeci, M. L., Massimino, D. & Nasca, M. R. Cutaneous vascular patterns in psoriasis. *Int. J. Dermatol.* **49,** 249–56 (2010).
46. He, D. *et al.* IL-17 and IFN-γ mediate the elicitation of contact hypersensitivity responses by different mechanisms and both are required for optimal responses. *J. Immunol.* **183,** 21463–21470 (2009).
47. Larsen, J. M., Bonefeld, C. M., Poulsen, S. S., Geisler, C. & Skov, L. IL-23 and T(H)17-mediated inflammation in human allergic contact dermatitis. *J. Allergy Clin. Immunol.* **123,** 486–492 (2009).
48. Cai, Y. *et al.* Pivotal role of dermal IL-17-producing γδ T cells in skin inflammation. *Immunity,* **4,** 596–610 (2011).
49. Mabuchi, T., Takekoshi, T. & Hwang, S. T. Epidermal CCR6+ γδ T cells are major producers of IL-22 and IL-17 in a murine model of Psoriasiform dermatitis. *J. Immunol.* **187,** 5026–5031 (2011).
50. Hedrick, M. N. *et al.* CCR6 is required for IL-23–induced psoriasis-like inflammation in mice. *J. Clin. Invest.* **119,** 2317–2329 (2009).
51. Zheng, Y. *et al.* Interleukin-22, a T(H)17 cytokine, mediates IL-23-induced dermal inflammation and acanthosis. *Nature.* **445,** 648–651 (2007).
52. Leonardi, C. L. *et al.* Efficacy and safety of ustekinumab, a human interleukin-12/23 monoclonal antibody, in patients with psoriasis: 76-week results from a randomized, double-blind, placebo-controlled trial (PHOENIX 1). *The Lancet.* **371,** 1665–1674 (2008).

53. Shigeta, A. *et al.* An L-selectin ligand distinct from P-selectin glycoprotein ligand-1 is expressed on endothelial cells and promotes neutrophil rolling in inflammation. *Blood* **13,** 4915–4923 (2008).
54. Meixner, A. *et al.* Epidermal JunB represses G-CSF transcription and affects haematopoiesis and bone formation. *Nat. Cell Biol.* **10,** 1003–1011 (2008).
55. Nakamura, Y. *et al.* Phospholipase Cdelta1 is required for skin stem cell lineage commitment. *EMBO J.* **22,** 2981–2991 (2003).
56. Dassule, H. R., Lewis, P., Bei, M., Maas, R. & McMahon, A. P. Sonic hedgehog regulates growth and morphogenesis of the tooth. *Development.* **127,** 4775–4785 (2000).
57. Bleul, C.C. & Boehm, T. BMP signaling is required for normal thymus development. *J. Immunol.* **175,** 5213–5221 (2005).
58. Kouchi, Z. *et al.* Phospholipase Cdelta3 regulates RhoA/Rho kinase signaling and neurite outgrowth. *J. Biol. Chem.* **286,** 8459–8471 (2011).

Acknowledgements

We thank Dr. Z. Kouchi, R. Fujimori, and Y. Hashimoto for technical assistances and fruitful discussions. We also thank Dr. T. Boehm for providing the *Foxn1* promoter construct. This work was supported by a Grant-in-Aid for Scientific Research (B), the Funding Program for Next Generation World-Leading Researchers, the Mochida Memorial Foundation for Medical and Pharmaceutical Research and the Takeda Science Foundation to K.F., as well as a Grant-in-Aid for Young Scientists (B) to Y.N. K. Kanemaru is supported by a predoctoral fellowship from the Japan Society of the Promotion of Sciences.

Author contributions

K. Kanemaru, Y.N., K.F. designed the experiments; K. Kanemaru, Y.N., K.S., R.K., S.T., M.Y., M.I., H.K., G.S., K. Kabashima and K.N. performed experiments; K. Kanemaru, Y.N., K.F., K.S., M.A., H.Y. and C.J. analysed data; K. Kanemaru, Y.N. and K.F. wrote the paper.

Additional information

Supplementary Information accompanies this paper at http://www.nature.com/naturecommunications

Competing financial interests: The authors declare no competing financial interests.

Reprints and permission information is available online at http://npg.nature.com/reprintsandpermissions/

How to cite this article: Kanemaru, K. *et al.* Epidermal phospholipase Cδ1 regulates granulocyte counts and systemic interleukin-17 levels in mice. *Nat. Commun.* 3:963 doi: 10.1038/ncomms1960 (2012).

Protection from liver fibrosis by a peroxisome proliferator-activated receptor δ agonist

Keiko Iwaisako[a,b], Michael Haimerl[a], Yong-Han Paik[a,c], Kojiro Taura[a], Yuzo Kodama[a], Claude Sirlin[b], Elizabeth Yu[d], Ruth T. Yu[d], Michael Downes[d], Ronald M. Evans[d,1], David A. Brenner[a], and Bernd Schnabl[a,1]

Departments of [a]Medicine and [b]Radiology, University of California at San Diego, La Jolla, CA 92093; [c]Department of Internal Medicine, Samsung Medical Center, Sungkyunkwan University School of Medicine, Seoul 135-710, Korea; and [d]Gene Expression Laboratory, Salk Institute for Biological Studies, La Jolla, CA 92037

Contributed by Ronald M. Evans, March 28, 2012 (sent for review November 18, 2011)

Peroxisome proliferator-activated receptor delta (PPARδ), a member of the nuclear receptor family, is emerging as a key metabolic regulator with pleiotropic actions on various tissues including fat, skeletal muscle, and liver. Here we show that the PPARδ agonist KD3010, but not the well-validated GW501516, dramatically ameliorates liver injury induced by carbon tetrachloride (CCl_4) injections. Deposition of extracellular matrix proteins was lower in the KD3010-treated group than in the vehicle- or GW501516-treated group. Interestingly, profibrogenic connective tissue growth factor was induced significantly by GW501516, but not by KD3010, following CCl_4 treatment. The hepatoprotective and antifibrotic effect of KD3010 was confirmed in a model of cholestasis-induced liver injury and fibrosis using bile duct ligation for 3 wk. Primary hepatocytes treated with KD3010 but not GW501516 were protected from starvation or CCl_4-induced cell death, in part because of reduced reactive oxygen species production. In conclusion, our data demonstrate that an orally active PPARδ agonist has hepatoprotective and antifibrotic effects in animal models of liver fibrosis, suggesting a possible mechanistic and therapeutic approach in treating patients with chronic liver diseases.

hepatic stellate cells | Kupffer cells | liver cirrhosis

Liver fibrosis is a common consequence of chronic liver injury including alcohol abuse, viral hepatitis, autoimmune disease, and nonalcoholic steatohepatitis. Chronic liver disease can progress to cirrhosis and hepatocellular carcinoma. Cirrhosis is a major health burden worldwide and currently is the 12th leading cause of death in the United States. Liver fibrosis is reversible if the causative agent (e.g., alcohol consumption, hepatitis B and C viral infections, or biliary obstruction) is removed successfully (1). However, the underlying causative agent is treated successfully only in subsets of patients with liver diseases, and there are no specific treatments for liver fibrosis. An ideal antifibrotic therapy would be liver specific, well tolerated when administered for prolonged periods of time, and effective in attenuating excessive collagen deposition without affecting normal extracellular matrix synthesis (2).

Peroxisome proliferator-activated receptors (PPARs) are members of the nuclear receptor family of ligand-activated transcription factors. They form heterodimers with retinoid X receptor (RXR) and bind to consensus DNA sites. Ligand binding induces a conformational change in PPAR–RXR complexes, releasing repressors in exchange for coactivators, and results in modulation of gene transcription. PPARs are able to transrepress as well as transactivate genes (3). Functional dissection of ligand-dependent coregulators of PPARs reveals that their transcriptional regulation is linked to histone modification and chromatin remodeling. All three subtypes of PPARs, including PPARδ, can be activated by fatty acids and fatty-acid derivatives. Based on studies using gene deletion and synthetic agonists, PPARδ is emerging as a key metabolic regulator. PPARδ agonists improve glucose and lipid homeostasis (4, 5) and increase skeletal muscle fatty-acid metabolism. PPARδ agonists have been shown to be exercise mimetics and to increase endurance in mice that already are undergoing exercise (6). PPARδ has anti-inflammatory activities, including inhibition of cytokine production and promoting the alternative activation of macrophages (7).

To determine whether PPARδ agonists are beneficial in experimental liver fibrosis, mice were treated orally with a PPARδ agonist, KD3010, or with the well-validated PPARδ agonist GW501516. Unexpectedly, KD3010, but not GW501516, showed hepatoprotective and antifibrotic effects in liver fibrosis induced by carbon tetrachloride (CCl_4) or bile duct ligation (BDL).

Results

PPARδ Agonist KD3010 Protects from Liver Injury. Liver injury was induced by repeated injections of CCl_4, and mice were treated daily with vehicle, the widely used PPARδ agonist GW501516 (6), or the PPARδ agonist KD3010 by oral gavage. Control oil-injected mice did not show any liver damage (Fig. 1*A*). Liver injury consisting of hepatocyte death and inflammation was seen in the vehicle- or GW501516-treated group injected with CCl_4 on H&E-stained liver sections but was markedly reduced in the KD3010-treated group (Fig. 1*A*). This result was confirmed by serum alanine aminotransferase (ALT) levels, which were reduced only in the KD3010 group compared with other groups (Fig. 1*B*). Both KD3010 and GW501516 induced PPARδ-responsive genes such as adipose differentiation-related protein (*ADFP*) and uncoupling protein 2 (*UCP2*), but not PPARα- and PPARγ-specific responsive genes such as *FGF21* and *CD36*, respectively (Fig. 1*C*).

KD3010-Treated Mice Show Less Hepatic Fibrosis. Fibrillar collagen deposition as a measure of liver fibrosis was determined by Sirius Red staining. Vehicle- or GW501516-treated animals showed bridging fibrosis. Fibrosis was lower in the KD3010 group (Fig. 1*D*) than in the other groups. The lower level of Sirius Red staining was confirmed by morphometric analysis (Fig. 1*E*). Hydroxyproline content, a measure for total collagen, was reduced in the KD3010 group (Fig. 1*F*). Mice subjected to CCl_4 and treated with KD3010 showed control levels of the inflammatory cytokine *TNFα* compared with the vehicle- and GW501516-treated groups (Fig. 1*G*). Similarly, α-smooth muscle actin (*αSMA*) mRNA, a marker of hepatic stellate cell activation, also was down-regulated in the KD3010 group. An

Author contributions: K.I., C.S., R.T.Y., M.D., R.M.E., D.A.B., and B.S. designed research; K.I., M.H., Y.-H.P., K.T., Y.K., and E.Y. performed research; K.I., C.S., R.T.Y., M.D., R.M.E., D.A.B., and B.S. analyzed data; and K.I., D.A.B., and B.S. wrote the paper.

The authors declare no conflict of interest.

Data deposition: The microarray data reported in this paper have been deposited in the Gene Expression Omnibus (GEO) database (accession code GSE32121).

[1]To whom correspondence may be addressed. E-mail: evans@salk.edu or beschnabl@ucsd.edu.

See Author Summary on page 7965 (volume 109, number 21).

This article contains supporting information online at www.pnas.org/lookup/suppl/doi:10.1073/pnas.1202464109/-/DCSupplemental.